Earth and Planetary Science Letters 301 (2011) 353–364

Contents lists available at ScienceDirect

Earth and Planetary Science Letters

journal homepage: www.elsevier.com/locate/epsl

Crustal compositions exposed by impact craters in the Tyrrhena Terra region of Mars: Considerations for Noachian environments

A. Deanne Rogers *

Department of Geosciences, Stony Brook University, 255 Earth and Space Sciences, Stony Brook, NY 11794-2100, United States

ARTICLE INFO

Article history:
Received 28 July 2010
Received in revised form 8 November 2010
Accepted 9 November 2010
Available online 9 December 2010

Editor: T. Spohn

Keywords:
Mars
composition
alteration
remote sensing
crater

ABSTRACT

Crater ejecta blankets distinguished by differences in thermophysical properties from the target material were investigated in Tyrrhena Terra, Mars. Approximately one third of craters exhibit spectral differences from target material in Mars Global Surveyor Thermal Emission Spectrometer (TES) data. Craters that exhibit these spectral differences from the target material do not strongly correlate with phyllosilicate exposures detected in near infrared data from the Compact Reconnaissance Imaging Spectrometer for Mars (CRISM). Shock processes cannot fully explain the observed spectral trends. Rather, the subtle spectral differences observed in TES data are likely due to differences in plagioclase and/or high-silica phase abundance relative to pyroxene abundance, with the crater ejecta exhibiting lower pyroxene abundance than target materials. These mineralogic trends are consistent with several scenarios, none of which can be ruled out from existing observations: 1) vertical variations in primary lithology (considered least likely), 2) subsurface alteration exposed by impact, 3) syn- or post-impact alteration associated with the impact process, such as devitrification of melt glass materials or alteration of highly shocked materials, and 4) light surface alteration that preferentially altered/removed plagioclase and/or high-silica glass relative to pyroxene and subsequent exposure of less-altered materials from the subsurface by impact. Scenario 2 is consistent with phyllosilicate detections; Scenarios 1, 3 and 4 are consistent with CRISM phyllosilicate detections in some impact craters if phyllosilicate mineral abundance is volumetrically small. Results from this work suggest that some signatures of alteration may be escaping detection by near infrared measurements; alteration environments would be best interpreted through a combination of near infrared and thermal infrared data sets, rather than near infrared detections alone.

1. Introduction

The driving reason for characterizing the composition, spatial distribution, diversity, and relative abundance of minerals on a planetary surface is to infer information about the history of magmatic and alteration processes on that body. Understanding the style and duration of alteration at both the surface and subsurface is a particularly important goal because these factors relate to ancient environments.

The Martian surface is dominated by loose or weakly cemented regolith (Christensen and Moore, 1992); however numerous small rock outcrops are scattered across the globe, usually exposed in craters and canyons (Edwards et al., 2009; Fergason et al., 2006). Remote spectroscopic measurements of Mars have revealed much information about the compositional diversity within both the surface layer regolith and in-place rock at a variety of spatial scales. Though the surface of Mars is largely basaltic, global-scale terranes may be distinguished on the basis of variations in olivine, pyroxene, feldspar and "high-silica phase" abundance (Poulet et al., 2009; Rogers and Christensen, 2007). In this work, "high-silica phase" refers to amorphous and/or poorly crystalline phases with Si/O>~0.35 (Michalski et al., 2005) and may include high-silica volcanic glass, secondary amorphous silica, zeolites, phyllosilicates, or poorly crystalline aluminosilicates such as allophane. Within these broad regions, hundreds of local-scale (10^2–10^3 m) concentrated exposures of olivine, pyroxene, sulfates, phyllosilicates, carbonate, iron oxides, high-silica deposits, and other hydrated silicates are observed (e.g., Bandfield, 2008; Ehlmann et al., 2009; Glotch and Rogers, 2007; Koeppen and Hamilton, 2008; Mustard et al., 2008).

These compositional variations provide insight into temporal and/or spatial changes in crustal formation processes or weathering regimes. For example, high-silica phases exhibit highest abundances (>30%) at latitudes >45°, suggesting an ice-related alteration process to concentrate silica at the surface (e.g., Rogers and Christensen, 2007; Wyatt et al., 2004). In equatorial regions, high-silica phases are typically present at ~15% areal abundance, also suggesting some degree of surface alteration (McDowell and Hamilton, 2009; Michalski et al., 2005). However, questions related to the pre-alteration surface composition and the degree of alteration remain unresolved.

* Tel.: +1 631 632 1509.
E-mail address: adrogers@notes.cc.sunysb.edu.

0012-821X/$ – see front matter © 2010 Elsevier B.V. All rights reserved.
doi:10.1016/j.epsl.2010.11.020

Though infrared spectroscopic measurements are only sensitive to the upper few hundred microns (or less) of a planetary surface, high-resolution imagers provide geomorphologic context that allows these mineral detections to be placed within a 3-dimensional stratigraphic framework. Indeed, many of these concentrated mineral detections are found in crater walls, canyons, and other quasi-vertical outcrop faces. An additional method of accessing subsurface mineralogy is to examine materials exposed by impact ejecta. For example, hundreds of phyllosilicate detections have been associated with impact materials (Mustard et al., 2008; Pelkey et al., 2007a). However, in general, studies of the subsurface via impact materials have been limited. In particular, thermal infrared data, which are highly sensitive to the abundance of minerals as well as surface thermophysical properties, have been under-utilized in studies of impact ejecta.

Using thermal infrared spectroscopic measurements, the spectral properties and bulk composition of impact ejecta blankets (EBs) from craters with diameters >1 km within the region of Tyrrhena Terra and Iapygia Terra, Mars (60–100°E, 0–30°S) were investigated. This study excluded impact-excavated material in crater walls and central uplifts mainly because these materials cannot be resolved in Thermal Emission Spectrometer (TES) data, for the smallest diameter craters in the desired sampling range. However, for large diameter craters (>30 km), systematic studies of central uplifts and crater walls are certainly achievable with TES data and should be the subject of follow-on work.

The study region, located between Syrtis Major and Hellas Basin, is primarily composed of Noachian-aged cratered plains with a few interspersed Hesperian-aged smooth units (Greeley and Guest, 1987). Intercrater surfaces in the region can be subdivided into two main subunits, which differ primarily in their olivine content, thermophysical properties, and overall morphology (Rogers and Fergason, submitted for publication). The olivine-enriched intercrater surfaces (Rogers and Fergason, submitted; Seelos et al., 2010), hereafter referred to as "Unit 2", are less degraded and exhibit higher thermal inertia than surrounding olivine-deficient surfaces ("Unit 1"), are estimated to vary between <100 m and <500 m in thickness, and are likely volcanic in nature (Rogers and Fergason, submitted). Here, it is shown that many of the crater ejecta blankets in this region exhibit differences in spectral properties, and likely bulk composition, from the surrounding target material. This paper explores the possible geological origins of the spectral differences and the implications for surface weathering and phyllosilicate formation in Noachian cratered terrains.

2. Data and methods

Though numerous craters are present in the Martian highlands, many of them have been subsequently modified by burial or erosion, via impact, fluvial and/or volcanic processes (Malin, 1976; Tanaka et al., 1988). Because the goal of this work is to spectrally sample subsurface materials via EBs, a method is needed to identify ejecta materials that are relatively unobscured by regionally derived sediment. To this end, Mars Odyssey Thermal Emission Imaging System (THEMIS) (Christensen et al., 2004) band 9 nighttime radiance images were used to identify craters whose EBs exhibit a thermal contrast from the surrounding plains (Fig. 1). Nighttime surface temperatures are primarily dependent on the thermal conductivity of the surface. On Mars, variations in thermal conductivity can be attributed primarily to variations in average particle size (e.g., rocks, sand, and dust) or degree of cementation (Kieffer et al., 1977). Depending on the competence of the target material, crater ejecta can be either rockier or less rocky than the surroundings; thus, crater ejecta can be either warmer or cooler than the surroundings in nighttime radiance data. A thermal contrast with respect to the surrounding area suggests that the EB has not been fully homogenized with regional materials through saltation, subsequent impact, or extensive surface chemical alteration. Thus, among all craters within the study region, those which have a discernable ejecta blanket in nighttime temperature images are those which are more likely to expose excavated material in spectral measurements. For this work, ejecta blankets were distinguished by visually inspecting the nighttime radiance mosaics for rayed patterns extending radially from the crater or lobate circular patterns surrounding the crater that extend for a distance greater than or equal to one crater diameter (e.g., Mouginis-Mark, 1979).

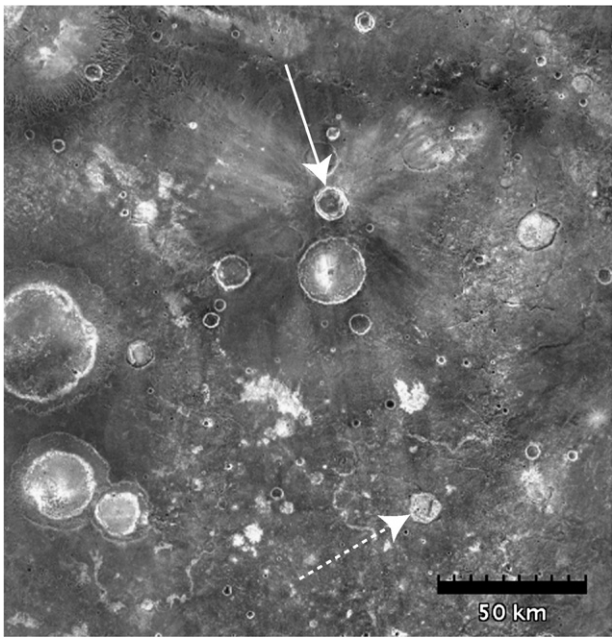

Fig. 1. Nighttime THEMIS radiance mosaic. Solid arrow points to a crater with thermally-distinct impact ejecta. Dashed arrow points to a crater of similar diameter, in which no ejecta blanket is discernible.

For each of these craters, TES emissivity spectra (Christensen et al., 2001) were extracted from 1) the EB and 2) surrounding target materials using the TES data query constraints of Rogers and Christensen (2007). Surrounding target materials were determined by finding the margin of the EB in the nighttime thermal radiance imagery, and selecting an adjacent surface outside of the EB that is covered by the same TES orbit(s) as the EB. It is possible that the surrounding target materials include ejecta material from the crater of interest or other craters, if those ejected materials have the same thermophysical signatures as the underlying target material. The broader region around each thermally distinct EB was closely examined for ejecta materials from nearby craters in an effort to avoid other EBs; however there may be cases where impact material was unknowingly included in the "surrounding" surface.

For each EB–target pair, atmospheric components were removed and surface emissivity spectra were compared to determine if there were spectral differences. To avoid interpreting spectral variations that might be attributed to minor inaccuracies in atmospheric correction, spectra were selected from the same TES orbit, where atmospheric changes between the two surfaces were likely to be minimal (e.g., Rogers et al., 2008). Where available, multiple orbits were examined for each pair. Atmospheric components were removed by modeling the emissivity with a library of atmospheric end-member and mineral spectra, using a linear least squares fitting routine (Bandfield, 2002; Bandfield et al., 2000a,b; Rogers and Aharonson, 2008). Atmospheric components were then scaled by their modeled concentrations and subtracted from the measured emissivity to produce surface emissivity; additional output from the least squares minimization included mineral abundances and

estimated standard errors on abundance (Bandfield, 2002; Rogers and Aharonson, 2008). In this work, the spectral library was similar to that used by Rogers et al. (2008), with the addition of anorthositic feldspars shocked at various pressures (Johnson et al., 2002) and the omission of micas and amphiboles.

All surface emissivity spectra were normalized to the average spectral contrast to highlight differences in spectral shape between surfaces and also between individual orbits. The spectral properties of each EB and target were evaluated to determine whether significant spectral differences are present between each EB–target pair member using the following two-step procedure. Step 1: Where at least two orbits were available for a given EB–target pair, the EB and target were considered spectrally separable if the emissivity bracketed by the minimum and maximum emissivity values of the set of derived EB spectra from all orbits and the set of derived target spectra from the same orbits did not overlap in at least two channels. The use of multiple orbits builds confidence in the derived spectral shape of both EB and target; however, for some craters, only one orbit was available. Thus the target pairs that met the criteria from Step 1 were used to determine separability of target pairs where only one orbit was available, as described in Step 2. Step 2: Surface emissivity ratios (e.g., Hamilton et al., 2003; Ruff and Christensen, 2002) of all EB–target pairs were calculated for each crater by 1) averaging the set of derived EB spectra from all orbits and averaging the set of derived target spectra from the same orbits, then 2) calculating the ratio of the EB average spectrum and the target average spectrum. Ratios from the qualifying EB–target pairs described in Step 1 were then averaged, and the standard deviation was calculated. Ratios from the one-orbit EB–target pairs that were higher than the mean ratio plus the standard deviation for two consecutive channels were then also considered statistically different. Using the mean plus the standard deviation, rather than just the mean, ensures that noise or other anomalous points in the one-orbit ratios did not promote those ratios to the "separable" category. This process of determining separability was validated by examining the derived mineral abundances for all EB–target pairs. No pair that was categorized as statistically unseparable showed a statistical separation in mineral abundance.

For EB–target pairs found to be significantly distinct, major mineral abundances derived from linear least squares modeling were compared in order to identify the major mineralogic differences between EB and target material. Though some EB–target pairs were found to be spectrally separable, derived mineralogic abundances for some of these craters were not separable. This is because there is lower uncertainty (lower statistical error) associated with modeled atmospheric components relative to modeled mineral components. This results in better precision in determination of surface spectral shape than in determination of composition. Thus for cases where the true differences in composition between surfaces are not extreme, such as with EB–target pairs in this work, it is possible to see a clear spectral distinction but not a clear mineralogical distinction. Finally, near infrared CRISM (Murchie et al., 2007) multispectral summary parameter images (Pelkey et al., 2007b; Seelos et al., 2007) were also used to identify mineralogic differences between EB and target materials.

3. Results

Sixty-three (63) craters within the study area have thermally distinct EBs in THEMIS nighttime radiance images. Of the EBs studied, 11 were not covered with enough TES data that fit the quality constraints (Section 2). Of the remaining 52, ~35% exhibit spectral differences from the surrounding target materials (Fig. 2A). The remaining EBs are not distinguished from their surroundings in thermal infrared spectral properties at coarse spatial scale. There is no apparent control on why some craters show spectral differences from the target surfaces, whereas others do not. There is no correlation of spectral properties with crater diameter (and thus excavation depth), nor does there appear to be a spatial/regional control (Fig. 2A). Composition of the target material also does not appear to be a factor, with ~50% of Unit 1 targets exhibiting a spectral difference from EBs and ~60% of younger Unit 2 targets exhibiting a spectral difference from EBs.

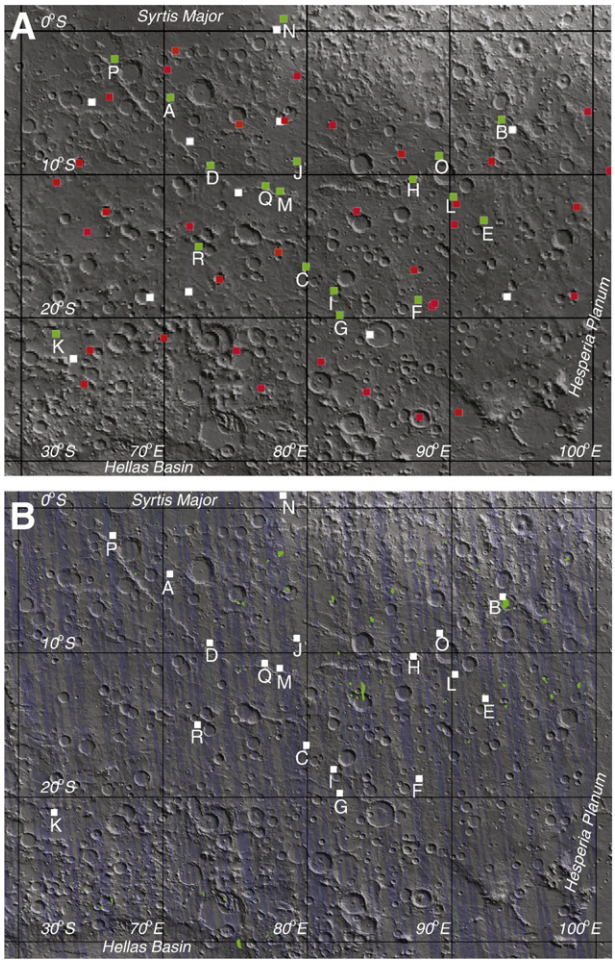

Fig. 2. A. Locations of thermally distinct ejecta blankets (EBs) in the study region. Green points indicate EBs that are spectrally distinguishable from the target material. Letters indicate crater labels shown in Table 1. Red points indicate EBs that are not spectrally distinguishable from the target material. White points indicate EBs with insufficient data that met quality constraints. Background is TES albedo draped on MOLA shaded relief. B. Rough location map of phyllosilicate mineral detections (green polygons) from CRISM 2.3 μm absorptions in multispectral survey data (e.g., Seelos et al., 2007). Blue shading shows multispectral survey coverage (~40%) at the time the map was created. Labeled white polygons represent EBs that are spectrally distinguishable from the target material, from panel A.

In general, the spectral differences between EB and target surface are consistent for each pair, and are largely observed in the ~435–507 cm^{-1} region, where EB materials exhibit a higher emissivity at ~507 cm^{-1} and lower emissivity at ~435 cm^{-1}, relative to target materials (Fig. 3). In fact, these spectral differences are so consistent that a spectral index map displaying the emissivity slope between ~502 and 470 cm^{-1} commonly highlights the crater ejecta clearly (Fig. 4). This spectral slope index (also known as the TES 465 cm^{-1} index) was developed by Ruff and Christensen (2007) to identify high-silica phases; however, as shown in Figure 5 it is also sensitive to changes in plagioclase/pyroxene ratio. Note that the most consistent and primary difference between craters and target materials is at low wavenumbers (<508 cm^{-1}); thus, typically the EBs are not distinguished from their target surfaces in THEMIS DCS images because THEMIS does not cover this low wavenumber region (Christensen et al., 2004).

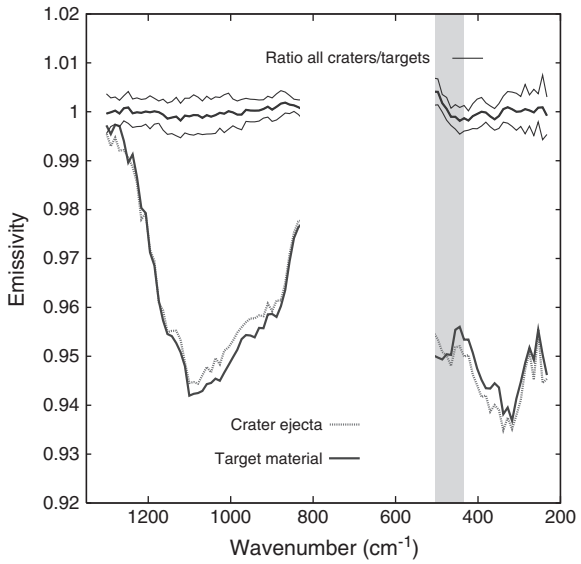

Fig. 3. Example TES surface emissivity spectrum from crater ejecta and surrounding target material. For all ejecta–target pairs that were found to be spectrally distinguishable, ratios of ejecta/target emissivity were averaged. Thin lines represent one standard deviation around the mean. Gray shaded area highlights the spectral region where differences between the pair members are observed.

Mineral abundance estimates were examined in detail for the 18 spectrally distinct EBs (Table 1). As described in Section 1 and in Rogers and Fergason (submitted), the intercrater surfaces in the Tyrrhena Terra region can roughly be divided into two compositional/thermophysical units: 1) older, less-mafic, degraded surfaces with relatively low thermal inertia (Unit 1), and 2) younger, more mafic, resistant surfaces with relatively higher thermal inertia (Unit 2). These units are distinguished with a TES spectral index near ~507 cm^{-1} as well as by morphology in THEMIS daytime radiance images (Rogers and Fergason, submitted). Unit 2 was estimated to vary between <100 and <500 m thick. For the following discussion of EB mineralogic composition, results are divided by target material. First, it should be noted that the average and range of derived mineral abundances for the two target types do not statistically separate in this work (Table 1, Fig. 6A). There is wide variability in the

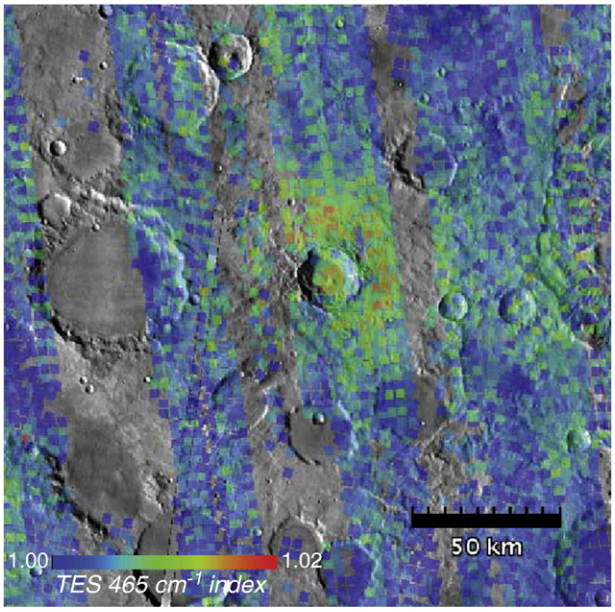

Fig. 4. TES 465 cm^{-1} index strength (Ruff and Christensen, 2007) overlaid on THEMIS daytime radiance mosaic. Center crater exhibits strong 465 index values in the crater floor and ejecta blanket.

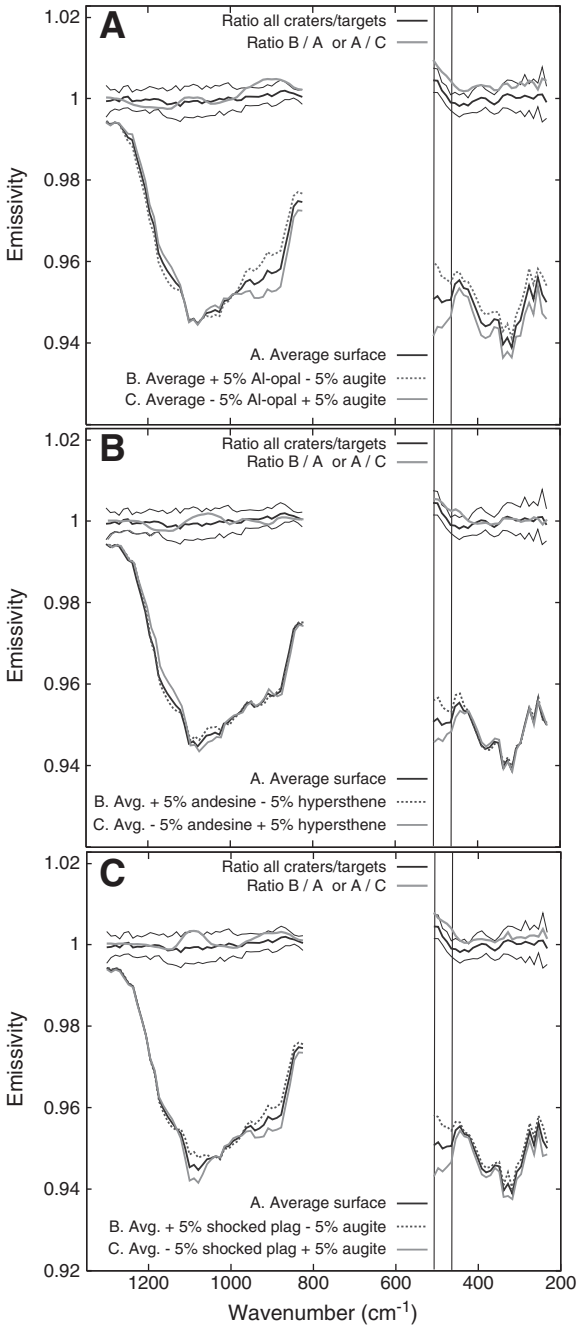

Fig. 5. Demonstration of the spectral changes to average Unit 1 intercrater plains arising from subtraction or addition of 5% pyroxene and addition or subtraction of 5% A) high-silica phase, B) plagioclase, and C) shocked anorthosite (~53 GPa). Ratios of the synthetic spectra to the average surface are compared with the average EB–target surface ratio ("Ratio all craters/targets") from Figure 3. The black vertical lines represent the spectral region of the TES 465 cm^{-1} index derived by Ruff and Christensen (2007). The 465 cm^{-1} index is sensitive to high abundances of high-silica phases but is also affected by changes in plagioclase/pyroxene ratio and changes in shocked plagioclase/pyroxene ratio.

derived mineral abundances for the Unit 2 target surfaces. There are two likely explanations for this. Less mafic materials (possibly sediment derived from Unit 1) are commonly observed overlying exposures of Unit 2; these materials are estimated to be quite thin in most areas because they do not strongly change the long wavelength (e.g., >15 μm) spectral character and the overall morphology is unchanged (Rogers and Fergason, submitted). However, in some cases these deposits are thick enough to change the derived mineralogy of the surface (Rogers and Fergason, submitted). Thus Unit 2 can be variable in surface composition because of these somewhat common overlying deposits. A second

Table 1
Derived mineral abundances for EB and target materials[a].

Crater label	A		B		C		D		E		F		G		H		I		J		K		L		M		N		O		P		Q		R		Avg. & Std. Unit 1 targets		Avg. & Std. Unit 2 targets	
Target type[b]	1		1		1		1		1		1		1		1		1		2		2		2		2		2		2		2		2		U					
D2300 detection[c]	ln peak		yes		no		n/a		yes**		n/a		no*		yes		no		n/a		no		no		no		n/a		no		no		n/a		no					
Ejecta																																									
Quartz	0	*0*	2	*1*	1	*1*	2	*1*	2	*1*	1	*1*	1	*1*	0	*1*	0	*0*	1	*1*	0	*0*	1	*1*	0	*0*	0	*1*	1	*1*	1	*1*	2	*1*	1	*1*	1	1	1	1
Feldspar	37	*3*	31	*3*	28	*4*	34	*4*	26	*5*	33	*6*	27	*4*	33	*6*	33	*5*	25	*4*	36	*6*	28	*5*	35	*6*	17	*5*	20	*5*	33	*6*	29	*4*	33	*4*	31	4	28	7
Pyroxene	23	*3*	22	*3*	28	*4*	26	*3*	19	*4*	23	*6*	24	*4*	20	*5*	23	*5*	29	*4*	31	*4*	31	*3*	23	*5*	38	*6*	25	*4*	17	*5*	26	*4*	23	*3*	23	3	27	6
Olivine	8	*3*	7	*2*	3	*2*	9	*2*	9	*3*	13	*4*	8	*3*	10	*3*	0	*3*	11	*3*	1	*2*	11	*3*	17	*5*	5	*4*	15	*3*	10	*2*	8	*3*	8	*3*	8	4	10	5
High-Si phases	21	*3*	24	*6*	23	*5*	19	*4*	28	*7*	20	*5*	23	*4*	25	*5*	27	*6*	20	*7*	19	*4*	20	*4*	20	*8*	17	*11*	22	*8*	23	*4*	21	*7*	20	*4*	23	3	20	2
Hematite	0	*2*	1	*2*	2	*1*	2	*1*	2	*2*	0	*0*	1	*2*	0	*0*	2	*2*	0	*2*	0	*0*	0	*0*	0	*0*	0	*0*	0	*0*	2	*2*	3	*1*	3	*2*	1	1	1	1
Sulfate	6	*2*	8	*2*	8	*1*	5	*2*	9	*2*	7	*3*	10	*2*	6	*2*	12	*2*	9	*2*	10	*2*	8	*2*	2	*2*	15	*2*	14	*2*	8	*2*	8	*2*	9	*2*	8	2	9	4
Carbonate	4	*1*	5	*1*	7	*1*	4	*1*	5	*1*	5	*1*	5	*1*	5	*1*	3	*1*	6	*1*	3	*1*	2	*1*	2	*1*	8	*1*	4	*0*	6	*1*	4	*1*	5	*1*	5	1	4	2
Target																																								
Quartz	0	*0*	0	*1*	0	*1*	1	*1*	1	*1*	2	*1*	1	*1*	0	*1*	0	*0*	1	*1*	0	*0*	1	*1*	0	*0*	0	*1*	1	*1*	1	*1*	2	*1*	0	*1*	1	1	1	1
Feldspar	31	*4*	32	*4*	26	*4*	28	*3*	27	*4*	27	*5*	24	*4*	23	*4*	33	*6*	31	*3*	48	*6*	22	*5*	15	*8*	15	*5*	20	*4*	24	*6*	30	*7*	24	*4*	28	3	25	11
Pyroxene	32	*3*	32	*4*	32	*4*	34	*3*	32	*3*	27	*4*	32	*4*	31	*3*	28	*6*	29	*3*	28	*4*	41	*4*	31	*9*	36	*5*	30	*3*	27	*5*	25	*6*	31	*3*	31	2	31	5
Olivine	8	*2*	7	*3*	7	*3*	10	*3*	7	*3*	15	*3*	9	*3*	11	*2*	2	*5*	5	*3*	6	*2*	13	*3*	24	*5*	6	*3*	13	*2*	10	*4*	9	*4*	6	*3*	8	3	11	6
High-Si phases	17	*3*	14	*7*	19	*6*	16	*4*	15	*4*	17	*5*	20	*7*	19	*3*	22	*7*	17	*6*	9	*4*	13	*6*	12	*3*	22	*9*	21	*6*	20	*8*	22	*8*	17	*6*	18	3	17	5
Hematite	0	*0*	3	*2*	0	*0*	1	*2*	3	*2*	0	*0*	0	*0*	0	*2*	1	*2*	3	*2*	0	*0*	0	*0*	0	*0*	0	*0*	0	*0*	1	*2*	0	*0*	4	*1*	1	1	0	1
Sulfate	9	*2*	9	*3*	10	*3*	7	*2*	9	*2*	9	*2*	9	*2*	11	*2*	11	*2*	10	*2*	8	*2*	7	*2*	13	*3*	15	*2*	13	*2*	11	*3*	8	*3*	13	*2*	9	1	10	3
Carbonate	4	*0*	4	*1*	5	*0*	3	*1*	5	*1*	4	*1*	5	*0*	4	*1*	3	*1*	4	*1*	2	*1*	4	*1*	5	*1*	7	*1*	3	*1*	6	*1*	4	*1*	5	*1*	4	1	4	2

*CRISM data coverage very sparse.
**Crater E shows elevated 465 and 530 cm^{-1} index values (Ruff and Christensen, 2007), possibly indicating phyllosilicate detection in TES data. Phyllosilicate minerals are not modeled above detection limits, however.
[a] The number in italics indicates standard error on de rived abundance.
[b] 1: Unit 1 target type. 2: Unit 2 target type. U: Dominant target surface is uncertain. See text for details.
[c] "yes": Coherent, elevated D2300 index values observed . "no": Elevated D2300 values not observed. "n/a": No data coverage. "in peak": Elevated D2300 values observed in central peak only.

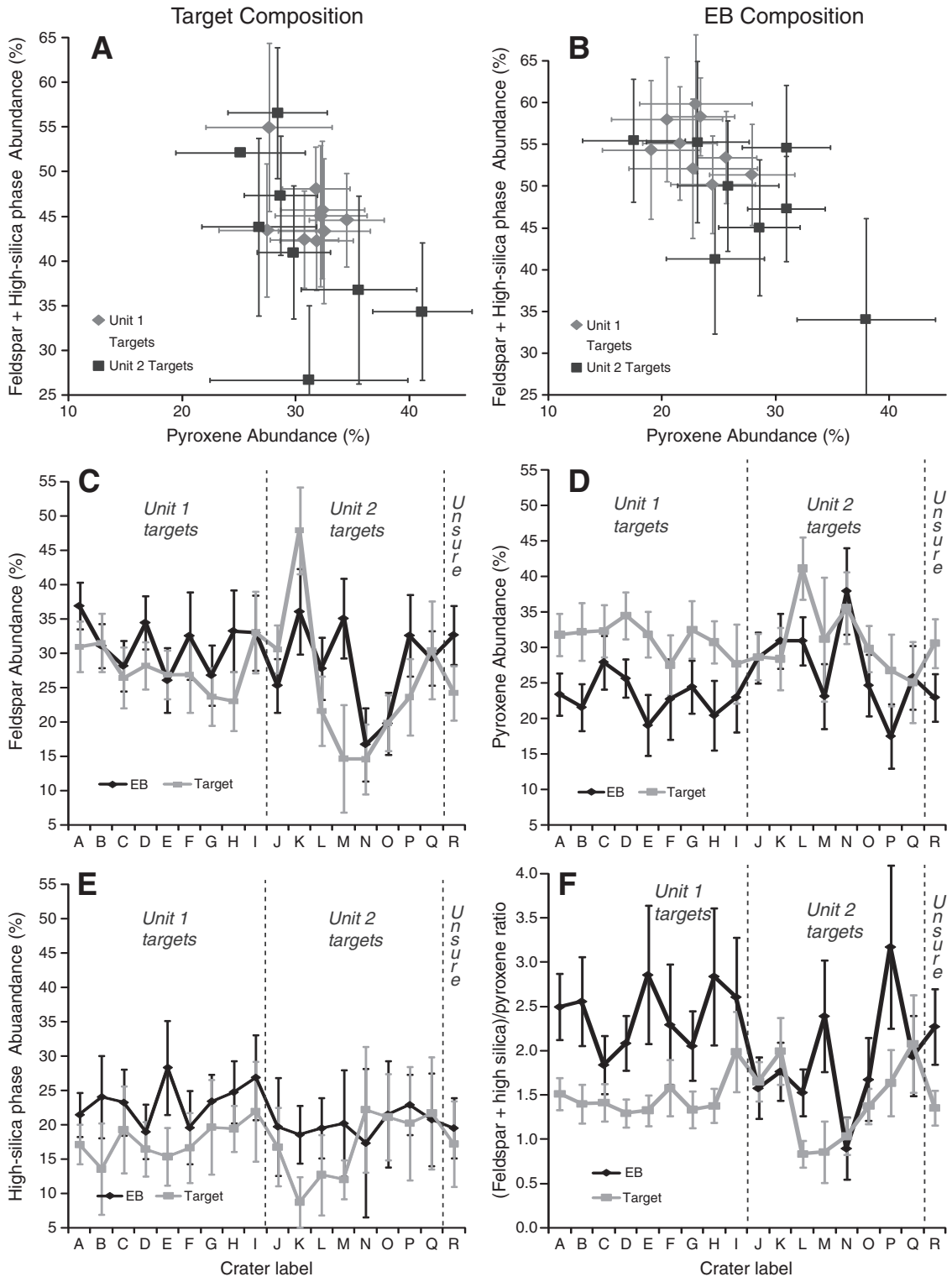

Fig. 6. A. Derived target compositions separated by unit type. B. Derived spectrally distinct EB compositions separated by unit type. C–E. Comparison of derived C. feldspar, D. pyroxene, and E. high-silica phase abundance for spectrally distinct EBs. F. Comparison of derived (feldspar + high-silica phase)/pyroxene ratio for spectrally distinct EBs.

explanation may be orbit-to-orbit variability in correction for atmospheric components (e.g. Rogers and Christensen, 2007) which can affect mineral abundance; however, this second possibility is likely a minor contributor to the variability and cannot account for all of the variation. The EBs do partially separate (Fig. 6B) depending on the target type, where in general, EBs associated with Unit 2 targets generally do show increased abundances of pyroxene (or olivine) and decreased abundances of feldspar and high-silica phases relative to EBs associated with Unit 1 targets. Thus to first order, the EBs reflect the overall mineralogic differences between the two major target types found in the region. The primary goal, however, is to evaluate differences between target and ejected materials. The most straightforward way to do this is to compare derived abundances for EB–target pairs for each individual crater, because the same orbit or set of orbits was used for each pair, thereby minimizing variability due to imperfections in the atmospheric correction process. Figure 6C–E shows differences in derived feldspar, pyroxene and high-

silica phase abundance for EBs and target materials for each crater. For the spectrally distinct EBs associated with Unit 1 targets, model results indicate that the spectral differences between EB and target are due primarily to decreased pyroxene abundance and increased feldspar and/or high-silica phase abundance in the EB relative to target material. For most craters, the modeled feldspar and high-silica phases for EBs and targets do not statistically separate, thus it is not clear if the decrease in pyroxene corresponds with higher abundance of feldspar, high-silica phases, or a combination of the two. However, it should be noted that if either high-silica phases or feldspars are excluded from the library, the surface spectra cannot be well-modeled, particularly in the ~435–507 cm^{-1} spectral region. To simplify, the differences between EBs and targets can be summarized by using a ratio of feldspar + high-silica phases to pyroxene (Fig. 6F), where EBs generally show an increased ratio relative to target materials. These trends are not as clear for Unit 2 targets (Fig. 6C–F); in some cases a higher (feldspar + high-silica)/pyroxene ratio is observed in the EB relative to target, whereas in other cases, a lower ratio is observed. Finally, in most EBs and targets, olivine is possibly present in minor abundances (5–10%), which is at or slightly above the detection limit for olivine established by Koeppen and Hamilton (2008). There is not a clear distinction in olivine abundance for most EB–target pairs. Phyllosilicate minerals are not modeled above detection limits (>15%) for any EB, but they might be contributors to the modeled high-silica phases.

Phyllosilicate mineral exposures in the study region were identified by mapping 2.3 μm absorption intensities, provided in CRISM multispectral survey D2300 parameter maps. Where spectrally distinct EBs were not covered by CRISM multispectral survey data or where elevated D2300 parameter values were not observed in spectrally distinct EBs, the CRISM database was also searched for targeted full or half resolution summary parameter images in an effort to increase spatial coverage or resolve small D2300 detections.

Spatially coherent D2300 parameter values exceeding 0.01 are shown in Figure 2B (example, Fig. 7A). As also discussed by Mustard et al. (2008) and Pelkey et al. (2007a), hundreds of phyllosilicate exposures are found in the region and are primarily associated with impact materials. There is no apparent relationship between phyllosilicate occurrence and elevated (plagioclase + high-silica)/pyroxene ratio occurrence; however, it should be noted that 5 of the 18 spectrally distinct EBs lack data coverage with the CRISM summary parameter or higher resolution targeted products, reducing the number of craters available for meaningful statistics. Three of the spectrally-distinct EBs contain detectable phyllosilicates whereas the other 10 EBs do not (Table 1; examples shown in Fig. 7). Where CRISM data were available, subtle differences in pyroxene VNIR summary parameter values between EB and target were observed in only half of the 18 spectrally distinct (in the thermal infrared) EB–target pairs. Thus there is a slight disconnect between the CRISM and TES measurements of pyroxene variability for the spectrally distinct craters; one would expect CRISM data to always show a decrease in pyroxene where TES detects a decrease in pyroxene, such as for the 18 spectrally distinct craters (Fig. 6D). This disconnect might be attributed to complicating effects from coatings on the target surfaces that are optically thin at thermal infrared wavelengths but thick at near infrared wavelengths; alternatively, there could be subtle particle size variations that affect the relative pyroxene strengths between pair components. In any case, it is a reminder of the subtlety of the spectral and compositional differences observed in the data sets.

Interestingly, four of the 63 thermally distinct craters show elevated D2300 parameter values but did not qualify as "spectrally distinct" EBs in TES data. These craters do show relatively strong TES 465 cm^{-1} index values (>1.01) in TES data. However, so do the surrounding target materials. Thus these craters did not show up as spectrally distinct from surroundings, using the criteria described in Section 2. It is not clear why these Unit 1 target surfaces have slightly stronger 465 cm^{-1} values than other Unit 1 target surfaces. It is possible that these areas experienced different alteration conditions to change the spectral character, or perhaps they consist of a higher fraction of ejected material from other craters (but do not show a thermal contrast). Similarly, Rogers and Fergason (submitted) report variable high-silica phase abundance within Unit 1, and note that there is no obvious correspondence with morphology.

4. Discussion

Detailed spectroscopic mapping indicates that approximately ~35% of EBs with a thermophysical contrast from their surroundings exhibit spectral differences from the impact target material. There is no apparent spatial, vertical or target material compositional control that gives rise to these spectral differences. This suggests that the process(es) that created or preserved the spectral differences varied in space and/or time. A likely explanation for the spatial variation is that some of the thermally distinct EBs have been homogenized enough with regionally-derived sediment(s) to obscure any spectral differences from the target material that may be present. It is important to note that though this study focused on craters whose ejecta blankets exhibit a thermal contrast from surroundings, TES

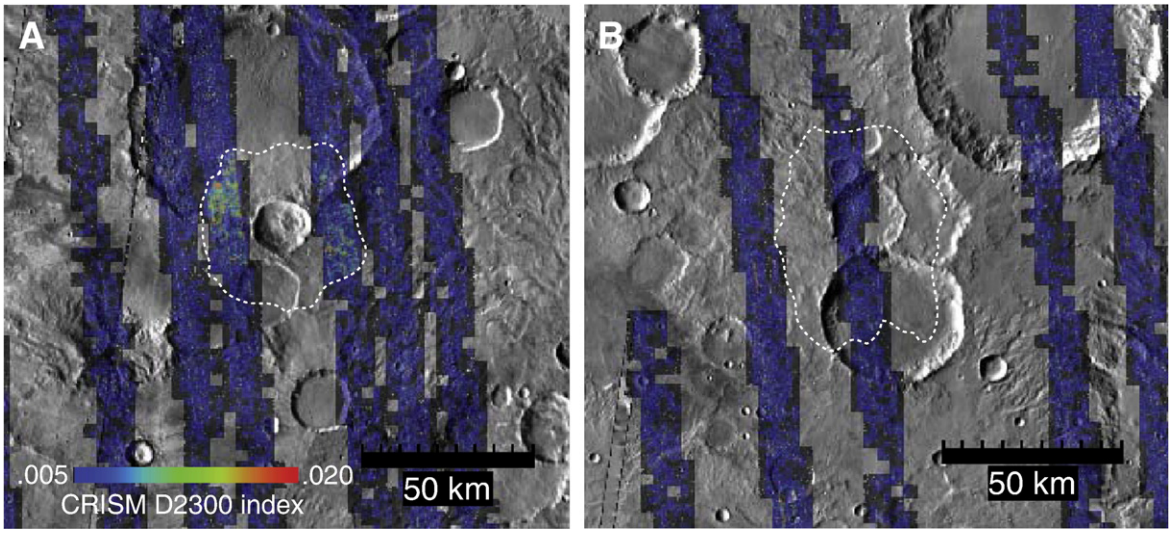

Fig. 7. CRISM D2300 index (2.3 μm absorption strength) from multispectral survey images, overlaid on THEMIS daytime radiance mosaic. Both images show thermally distinct crater ejecta that are also spectrally distinct from the target material. A) Crater ejecta with strong 2.3 μm absorption. B) Crater ejecta blanket that lacks 2.3 μm absorption. Both figures represent data coverage at time of writing.

465 cm^{-1} index maps highlight several craters in the region despite the lack of a thermal contrast. Thus the presence/absence of a thermal contrast is not a strict indicator of minimal obscuration by regionally derived sediments.

Explanations for the spectral differences can be initially divided into two categories: 1) shock deformation of target material during impact (in other words, structural differences only), or 2) true compositional differences between the EB and target material, either from stratigraphic variations in primary lithology or by some alteration process at the surface or subsurface. Changes in mineral structure are known to occur from high shock pressures (Ahrens and Rosenberg, 1966) and are evident in thermal infrared spectra of shocked vs. unshocked materials (e.g., Johnson et al., 2007); within basaltic materials, feldspars are much more susceptible to shock during impact than pyroxenes (Johnson et al., 2007). At very high shock pressures (e.g., ~20–25 GPa), emission features of basaltic materials broaden and shift due to higher abundance of diaplectic glass occurrence within plagioclase. In fact, the glass-like appearance of highly shocked feldspars led Johnson et al. (2002) to suggest that shocked plagioclase might account for at least part of the "high-silica phase" component observed in TES data of many surfaces. To determine if shocked materials might be responsible for the spectral differences between EBs and target materials, increasing percentages of the thermal emission spectra of shocked basalts (Johnson et al., 2007) (~30 and ~53 GPa) were mathematically mixed with unshocked basalt (Fig. 8). To mimic the overall spectral differences between EB and target materials, particularly in the ~508–450 cm^{-1} spectral region, a minimum of 30% of basalt shocked at ~53 GPa or 55% of basalt shocked at ~30 GPa must be added to unshocked basalt. Outside of the ~508–450 cm^{-1} spectral range, however, these mixtures do not closely reproduce the EB–target spectral differences, within error (Fig. 8). Mixtures of unshocked basalt and basalts shocked at pressures <30 GPa could not reproduce the observed EB–target spectral differences within any part of the spectral range. Addition of only 5% of highly shocked anorthosite to the average Unit 1 target surface does reproduce the observed trends (Fig. 5C). However, this scenario implies 5% of pure shocked plagioclase, not 5% of basalt which contains shocked plagioclase. Thus, whether comparing shocked basalt mixtures or comparing mixtures of target materials and shocked plagioclase, both imply large percentages (>30%) of highly shocked material. As noted by French (1998, Chapter 3), only a small percentage of the transient crater volume experiences shock pressures in excess of 30 GPa during impact. The high fraction of highly shocked materials needed to reproduce the observed spectral trends makes it difficult to support this explanation as the only source of spectral differences observed.

If the spectral differences are compositional in nature, spectral models of the EB–target pairs indicate that those differences are characterized by, for most craters, enrichment in plagioclase and/or high-silica phases, and deficiency in pyroxene, in EBs relative to the target material (Fig. 6C–F). These trends are true for all of the Unit 1 targets, but only true for some of the Unit 2 targets. Craters J, K, N, and Q do not follow these trends. The EB for crater J is primarily distinguished from target material by its olivine abundance, where the EB is enriched in olivine by ~5% relative to target material (Table 1). This may represent a case where the target material contained overlying thin olivine-deficient deposits (see Rogers and Fergason, submitted, or the description of these occurrences in Section 3). Or, the olivine enrichment may be due to excavation of an olivine-rich unit that is unique to the area surrounding that particular crater. Target material for crater K shows a much larger feldspar abundance than typical for any of the targets (Table 1), and may represent a unique unit in the region. Target materials for craters N and Q do not show statistically separable differences from EB materials in any grouped mineral abundance (Table 1), but are distinguished by their modeled plagioclase solid solution compositions. Each of these four craters represents a special case that could have one or more explanations that are distinct from the majority of craters. These four craters are difficult to evaluate in the context of the other craters and are not discussed further. It is noteworthy and relevant, however, that all of the Unit 1 EB–target pairs show a consistent trend in mineral abundance.

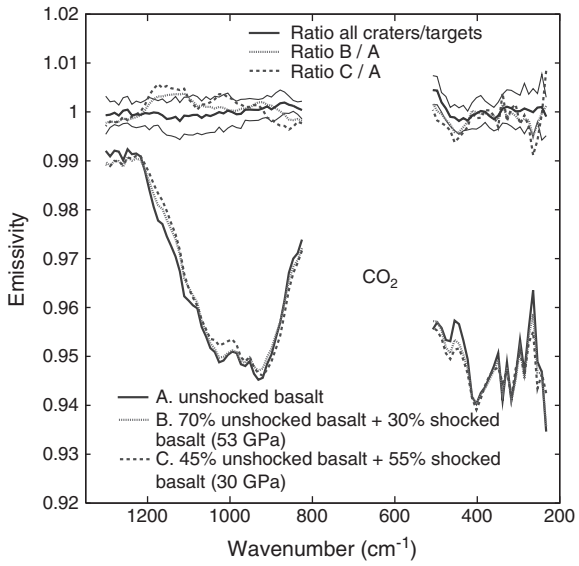

Fig. 8. Demonstration of the spectral changes associated with mixing shocked basalt and unshocked basalt. All laboratory spectra were acquired by Johnson et al. (2007). Synthetic spectra of unshocked basalt mixed with 30% shocked basalt (53 GPa) and 55% shocked basalt (30 GPa) are shown. Ratios of the synthetic mixture spectra (B and C) to the unshocked basalt (A) are compared with the average EB–target surface ratio ("Ratio all craters/targets") from Figure 3. Addition of a significant fraction of shocked basalt to unshocked materials produces a steepening of the emissivity slope between ~507 and 450 cm^{-1}, similar to that observed between the EB–target pairs of this study. However, ratios do not match well to the Mars observations outside of this spectral region.

The following four scenarios are offered to explain the mineralogical differences observed between EB–target pairs in Unit 1 targets: 1) vertical changes in lithology, 2) alteration in the subsurface, then subsequent exposure by impact, 3) post-impact alteration of shock-deformed materials including impact glass or high-pressure phases, or 4) surficial alteration of target material, then subsequent exposure of less-altered material by impact. The Unit 2 targets are discussed in the context of each scenario.

It is difficult to distinguish between these scenarios based solely on differences in mineralogical composition between the impact and surrounding materials. Though pyroxene, a primary mineral, differs fairly consistently for most target pairs, plagioclase and high-silica phase abundances do not separate between EBs and targets as well as pyroxene abundance does (Fig. 6). If either plagioclase or high-silica phases are excluded from the library, adequate fits to the EB or target surface spectra cannot be achieved (Section 3). This clearly indicates that both phases are present in both EBs and targets; however, the *differences* in relative abundance between EBs and targets are not statistically separable for most craters. Thus there is uncertainty about which phases (feldspar or high-silica phases or both) are actually changing with pyroxene abundance. Further uncertainty comes from the non-unique interpretation of "high-silica phases"; as described in Section 1, these phases may represent primary glass or alteration phases or a combination of both (though alteration phases are more likely (e.g., Michalski et al., 2005)). These observations are important because it is not clear if the main cause of spectral differences between the impact and surrounding materials is due to the relative abundance of primary minerals alone, or if the relative abundance of alteration phases (represented as "high-silica phases") is also changing. Furthermore, alteration processes could produce differences in

relative abundance of primary minerals (e.g., via mineral dissolution) but leave little trace of secondary/precipitated minerals, depending on post-alteration transport and modification processes (e.g., Bandfield and Rogers, 2008; Hurowitz et al., 2005). Thus arguments for/against each scenario below are based primarily on geologic context and reasoning rather than mineralogical composition alone. None of the following scenarios can be ruled out using existing observations; and, it is possible (even likely) that multiple processes have contributed to the observed spectral trends.

4.1. Vertical variations in primary lithology

There are numerous examples of vertical crustal heterogeneity on Mars; in some cases, stratigraphic sequences are observed over distances of hundreds of kilometers (e.g., Edwards et al., 2008; Griffes et al., 2007; Rogers et al., 2005). One scenario for the observations presented here is that the spectrally distinct EBs are exposing a pyroxene-poor lithology that underlies a pyroxene-abundant lithology (Fig. 9A). In this scenario, the spectral differences are due to differences in primary lithology only, with no preferential influence from alteration in either unit. In this scenario, the mafic intercrater plains surfaces (Unit 2) could represent similar materials, but exposed at the surface, where olivine- and/or pyroxene-enriched material is overlying a less mafic primary lithology. The smallest craters examined in detail in this study are 3 km in diameter, some of which do show spectral differences from the target material. Thus if this scenario is correct, the smallest spectrally distinct crater diameters indicate that an overlying pyroxene-enriched lithology must be less than 300 m thick in some areas (assuming the craters excavate to a depth of one-tenth the diameter [e.g., French, 1998]). An upper layer of spectrally distinct material is never observed in crater walls or other vertical exposures in this study region; however, this would be difficult to spatially resolve in TES data for many of the craters studied. Nevertheless, this scenario is considered the least likely because, assuming no drastic differences in unit thickness, the overlying pyroxene-enriched unit would constitute a larger proportion of the volume excavated by smaller craters. Therefore one would expect the spectral differences (and derived mineralogical differences) between EB and targets to be more pronounced with smaller crater diameters, and less pronounced with larger crater diameters. No such difference with crater diameter is observed.

4.2. Subsurface alteration exposed by impact

In this scenario, both Units 1 and 2 overlie an altered subsurface, and impacts excavated altered crust from beneath both surfaces

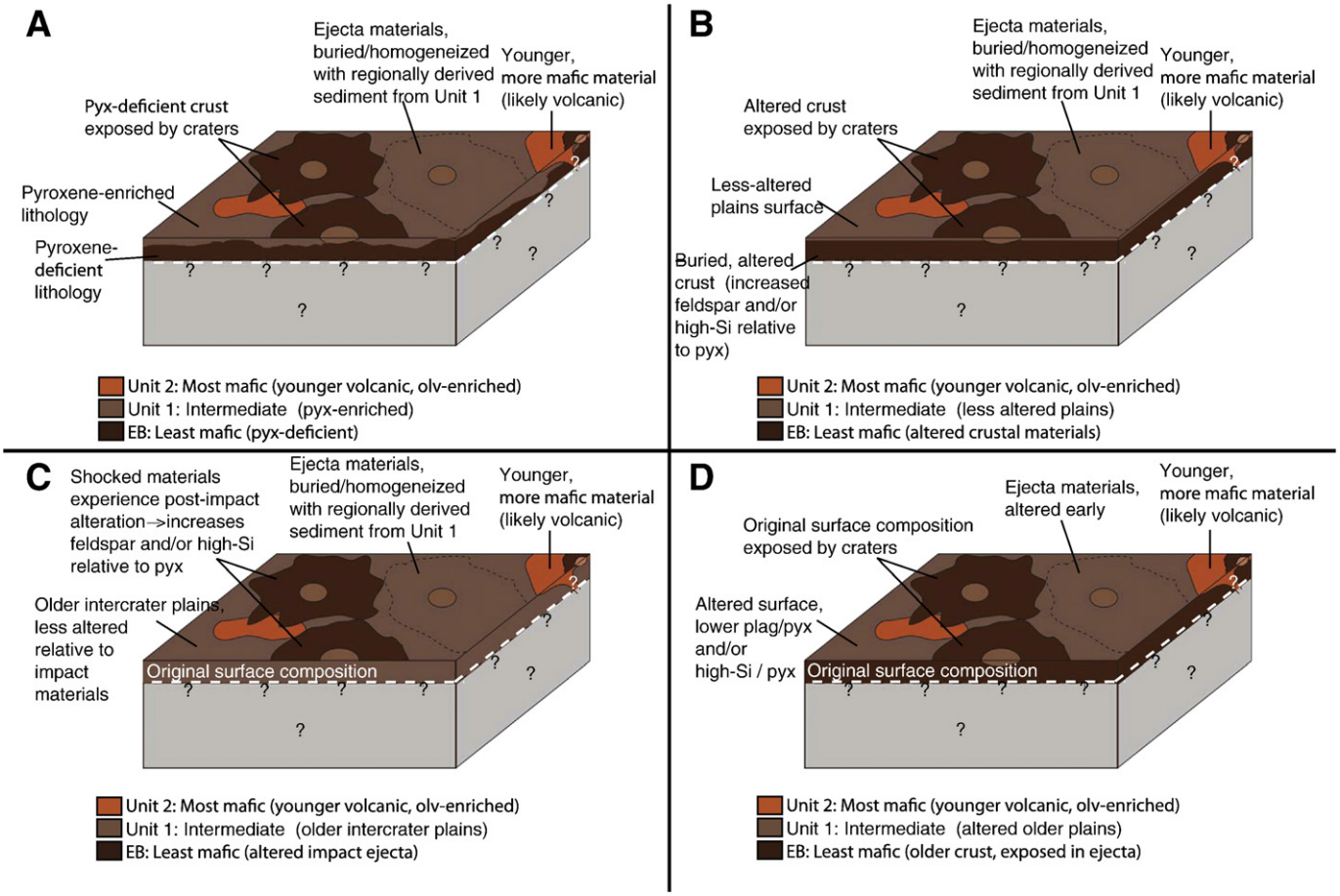

Fig. 9. Cartoon depictions of proposed scenarios to explain observed spectral trends. A. Scenario 1: A pyroxene-enriched unit of variable thickness overlies a pyroxene-deficient unit. Olivine-enriched Unit 2 rocks are emplaced volcanically in isolated locations within the region. Impacts into the pyroxene-enriched surfaces and Unit 2 expose pyroxene deficient materials from underneath. B. Scenario 2: Older crustal materials are altered via aqueous processes, decreasing the pyroxene abundance. (Note that the alteration could have been spatially variable; not uniform throughout the region as depicted here.) The altered materials are thinly buried with pyroxene-enriched, less altered sediments (Unit 1). Olivine-enriched Unit 2 rocks are emplaced volcanically in isolated locations within the region. Impacts into both Units 1 and 2 subsequently expose the pyroxene-deficient altered crust in ejecta blanket materials. C. Scenario 3: Shocked materials in EBs are more susceptible to alteration than surrounding target surfaces (Units 1 and 2). Alteration results in formation of high-silica phases, increasing the relative of abundance of high-silica phases to pyroxene in ejecta blanket materials relative to target surfaces. D. Scenario 4: Older crustal composition experienced light surface alteration to decrease the plagioclase abundance relative to pyroxene, creating Unit 1. Later volcanism partially fills intercrater plains and some crater floors (Unit 2); magma compositions are more mafic than older crust-forming magmas (original Unit 1). Later impacts exposed less-altered, primary compositions from the subsurface.

(Fig. 9B). The alteration process depleted pyroxene relative to feldspar and likely increased the abundance of high-silica phases. EBs in Unit 2 contain some proportion of Unit 2 material, hence the overall distinction between EBs of each target type (Fig. 6B). The suggestion that the subsurface was altered prior to impact is consistent with an existing framework for understanding the CRISM/OMEGA hydrated silicate detections associated with impact structures/materials. Numerous hypotheses have been put forth to explain the hydrated silicates; these range from pedogenic origins to hydrothermal systems (e.g., Ehlmann et al., 2009; Murchie et al., 2009; Mustard et al., 2008; Tornabene et al., 2007). It is possible that the decreased pyroxene abundance observed in excavated materials is related to the same process which formed the phyllosilicates. The spatial distribution of the spectrally unique craters and the lack of correlation with crater diameter would imply that whatever process occurred was widespread across a very large area, at all depths sampled by the craters. This likely rules out a hydrothermal system (if one wants to invoke only a single explanation for all spectrally distinct craters). Groundwater interactions could potentially lead to subsurface alteration over a large area; however, global hydrological models suggest that a water table would not have been at a consistently shallow depth throughout the entire study area (Andrews-Hanna et al., 2010). This leaves alteration by surface waters, followed by burial (e.g., Michalski and Dobrea, 2007), as the most likely explanation in this category.

The spatial distribution of spectrally unique craters contrasts with that of the phyllosilicate detections in this area (Fig. 2B), where there appears to be some regional control on the presence/preservation of phyllosilicate minerals. It is possible that both the near infrared observations of phyllosilicates and thermal infrared observations of pyroxene-deficient material are due to the same process (alteration), and the lack of coincident occurrences is due either to 1) variation in degree of alteration or 2) non-detection of phyllosilicate minerals in some of the spectrally unique (in the thermal infrared) craters. In either case, if the mineralogical differences observed in the TIR are related to alteration, the implications are that some signatures of alteration may be escaping detection by near infrared measurements, and that interpretations of alteration environments of phyllosilicate minerals should not rely too heavily on geographic distribution.

4.3. Alteration of shock-deformed materials

Shocked materials are more susceptible to alteration relative to unshocked materials, and post-impact alteration processes associated with ejecta blanket materials include devitrification of melt glasses and formation of hydrated silicate alteration products (Tornabene et al., 2007). Alteration associated with both of these processes would likely form clay minerals or poorly-crystalline high-silica phases (Fig. 9C). The apparent differences in mineralogy between some EB–target pairs are consistent with this explanation. In some cases, EB–target pairs where phyllosilicate minerals are detected might represent the more extreme form of alteration.

4.4. Exposure of less-altered materials by impact

The last scenario is that the uppermost surface of the Unit 1 target materials was lightly altered prior to impacts that exposed the EBs by partial and preferential dissolution of olivine, high-Si glass and/or plagioclase, resulting in an apparent enrichment of pyroxene relative to less altered materials excavated by impact. During or after this alteration period, Unit 2 was emplaced. Subsequent impacts exposed more pristine crust from beneath both surfaces (Fig. 9D). At first glance, one might suggest that this scenario be rejected on the basis of phyllosilicate detections in crater materials, which likely imply alteration of excavated materials rather than target surfaces (e.g., Section 4.2). However, it is possible that the phyllosilicates in crater ejecta and the plagioclase and/or high-silica phase deficiency in target materials represent two separate alteration processes. For example, though buried altered crust is suggested from phyllosilicate-bearing impact materials, surficial alteration associated with acidic fluids and low water-to-rock ratios is also implicated from observations elsewhere on Mars. There is evidence that olivine dissolution has been a prominent and widespread process in Martian history (Bandfield and Rogers, 2008; Bandfield et al., in press; Hurowitz et al., 2005; Tosca et al., 2004); geochemical arguments suggest that fluids involved in olivine dissolution were likely acidic and involved low water-to-rock ratios (Hurowitz and McLennan, 2007). Interaction of volcanic acidic volatiles with water vapor (the “acid fog” model) could produce these weathering conditions (Banin et al., 1997; Tosca et al., 2004).

The susceptibility of mineral dissolution in basalt is highly dependent on the mineral composition, fluid chemistry and pH, and the size of the mineral grains (e.g., Hurowitz et al. 2005; Keller, 1955; Loughnan, 1969; McAdam et al., 2006, 2008; Schott and Berner, 1984). For example, Ca-plagioclase is more susceptible than pyroxene, which is more susceptible than Na-plagioclase (glass and olivine are more susceptible than all of these materials) (e.g., Colman, 1982; Eggleton et al., 1987). Thus, a variety of factors could give rise to a decrease in feldspar in the target surface relative to subsurface materials; and the acidic, low water-to-rock ratio, surficial style of weathering could be entirely consistent with the observations presented here. Olivine is present in ~10% (average) abundance for excavated and target materials for both target types. However, the presence/absence of olivine does not help to constrain the problem, because the primary olivine abundance of crust forming materials is unknown. Furthermore, the uncertainties regarding 1) which phases (plagioclase and/or high-silica phases) are changing with pyroxene abundance and 2) the nature of the high-silica phases (glass vs. secondary phases) also complicate the ability to discount this scenario. If an increase in high-silica phases with decreasing pyroxene could be more confidently identified in EBs, this observation would likely rule out this scenario. This is because amorphous and/or poorly crystalline silicate phases are common secondary products produced during dissolution of basaltic minerals (e.g., Tosca et al., 2004); thus clear identification of increased high-silica phases in EBs would likely point to a more-altered subsurface rather than a more-altered target surface (the second scenario, Section 4.2).

If one considers that the phyllosilicate minerals could be volumetrically small and/or that they could have been formed in restricted zones/conduits in the subsurface, it is possible to reconcile the possibility of two separate alteration processes being represented in the near infrared and thermal infrared measurements. Phyllosilicate formation may have occurred at depth, or, at the surface prior to burial by materials that lack phyllosilicates, and was more regionally constrained (Fig. 2B); whereas plagioclase depletion could have occurred through widespread surficial alteration under acidic conditions and low water-to-rock ratios. The mineralogical trends between EB and target material as well as the spatial distribution of spectrally unique craters are consistent with this proposed scenario. Additionally, the lack of correlation with phyllosilicate detections may support this hypothesis over Scenario 2 (though the discrepancies in distribution could be related to discrepancies in preservation rather than formation mechanism).

This surficial weathering would have initiated early in Martian history, prior to subsequent impacts. Partial dissolution of surficial materials may have contributed to the formation of poorly-crystalline silicate phases that are typically modeled in TES and Mini-TES data (e.g., Glotch et al., 2006; McDowell and Hamilton, 2009; Michalski et al., 2005; Rogers and Aharonson, 2008) and may also have contributed to regolith development on early Mars. If these materials have experienced less alteration than the surface layer, the bulk compositions extracted from these craters are more representative of the primary composition of the upper crust-forming material.

5. Conclusions

Spectral differences are observed in approximately ~35% of EBs with a thermal contrast from surroundings in the Tyrrhena Terra region. These spectral differences cannot be entirely explained by shock processes. Rather the spectral trends must be due in part to mineralogic differences, where EBs are enriched in plagioclase and/or high-silica phases, and deficient in pyroxene relative to target materials. These mineralogic trends are consistent several scenarios, none of which can be ruled out from existing observations: 1) vertical variations in primary lithology (considered the least likely, Section 4.1), 2) subsurface alteration exposed by impact, 3) syn- or post-impact alteration associated with the impact process, such as devitrification of melt glass materials or alteration of highly shocked materials, and 4) light surface alteration that preferentially altered/removed plagioclase and/or high-silica glass relative to pyroxene and subsequent exposure of less-altered materials from the subsurface by impact. Scenario 2 is consistent with phyllosilicate detections; Scenarios 1, 3 and 4 are consistent with phyllosilicate detections in some impact craters if phyllosilicate mineral abundance is volumetrically small. Distinguishing between these scenarios may be difficult; however, targeted, detailed studies of variations in bulk composition associated with phyllosilicate-bearing and non-phyllosilicate-bearing crater materials may provide some insight. Finally, it is possible (maybe likely), that multiple processes have contributed to the observed spectral trends, and may explain the lack of spatial control on the presence of pyroxene-poor materials in thermally distinct EBs.

Three of the four scenarios involve alteration, and that these possible alteration signatures are not usually detected in the near infrared data. This suggests that alteration environments would be best interpreted through a combination of near infrared and thermal infrared data sets, rather than near infrared detections alone.

Acknowledgments

This work was supported by NASA Mars Data Analysis Program grant NNX08AL10G. I thank the JMARS development team at Arizona State University and the CRISM multispectral summary parameter image development team for straightforward and highly useful products. I am very grateful to Bethany Ehlmann and Vicky Hamilton for thorough and constructive reviews. Josh Bandfield and Tim Glotch provided thoughtful comments on an early version of the manuscript.

References

Ahrens, T.J., Rosenberg, J.T., 1966. Shock Metamorphism of Natural Materials. In: French, B.M., Short, N.M. (Eds.), Conference on Shock Metamorphism of Natural Materials. Mono Book Corp, Baltimore, MD.

Andrews-Hanna, J.C., Zuber, M.T., Arvidson, R.E., Wiseman, S.M., 2010. Early Mars hydrology: Meridiani playa deposits and the sedimentary record of Arabia Terra. J. Geophys. Res. 115, E06002. doi:10.1029/2009JE003485.

Bandfield, J.L., 2002. Global mineral distributions on Mars. J. Geophys. Res. Planets 107, 5042.

Bandfield, J.L., 2008. High-silica deposits of an aqueous origin in western Hellas Basin, Mars. Geophys. Res. Lett. 35, L12205.

Bandfield, J.L., Rogers, A.D., 2008. Olivine dissolution by acidic fluids in Argyre Planitia, Mars: evidence for a widespread process? Geology 36, 579–582.

Bandfield, J.L., Christensen, P.R., Smith, M.D., 2000a. Spectral data set factor analysis and end-member recovery: application to analysis of Martian atmospheric particulates. J. Geophys. Res. Planets 105, 9573–9587.

Bandfield, J.L., Hamilton, V.E., Christensen, P.R., 2000b. A global view of Martian surface compositions from MGS–TES. Science 287, 1626–1630.

Bandfield, J.L., Rogers, A.D., Edwards, C.S., in press. The role of aqueous alteration of Martian soils. Icarus. doi:10.1016/j.icarus.2010.08.028.

Banin, A., Han, F.X., Kan, I., Cicelsky, A., 1997. Acidic volatiles and the Mars soil. J. Geophys. Res. Planets 102, 13341–13356.

Christensen, P.R., Moore, H.J., 1992. The Martian surface layer. In: Kieffer, H.H., Jakosky, B.M., Snyder, C.W., Matthews, M.S. (Eds.), Mars. University of Arizona Press, Tuscon, AZ, pp. 686–729.

Christensen, P.R., Bandfield, J.L., Hamilton, V.E., Ruff, S.W., Kieffer, H.H., Titus, T.N., Malin, M.C., Morris, R.V., Lane, M.D., Clark, R.L., Jakosky, B.M., Mellon, M.T., Pearl, J.C., Conrath, B.J., Smith, M.D., Clancy, R.T., Kuzmin, R.O., Roush, T., Mehall, G.L., Gorelick, N., Bender, K., Murray, K., Dason, S., Greene, E., Silverman, S., Greenfield, M., 2001. Mars Global Surveyor Thermal Emission Spectrometer experiment: investigation description and surface science results. J. Geophys. Res. Planets 106, 23823–23871.

Christensen, P.R., Jakosky, B., Kieffer, H.H., Malin, M.C., McSween, H.Y., Nealson, K., Mehall, G.L., Silverman, S.H., Ferry, S., Caplinger, M., Ravine, M., 2004. The Thermal Emission Imaging System (THEMIS) for the Mars 2001 Odyssey Mission. Space Sci. Rev. 110, 85–130.

Colman, S.M., 1982. Chemical weathering of basalts and andesites. Evidence from Weathering Rinds. Geological Survey, U. S. Dept of the Interior, Washington, p. 51.

Edwards, C.S., Christensen, P.R., Hamilton, V.E., 2008. Evidence for extensive olivine-rich basalt bedrock outcrops in Ganges and Eos chasmas, Mars. J. Geophys. Res. 113, E11003.

Edwards, C.S., Bandfield, J.L., Christensen, P.R., Fergason, R.L., 2009. Global distribution of bedrock exposures on Mars using THEMIS high-resolution thermal inertia. J. Geophys. Res. Planets 114, E11001. doi:10.1029/2009JE003363.

Eggleton, R.A., Foudoulis, C., Varkevisser, D., 1987. Weathering of basalt — changes in rock chemistry and mineralogy. Clays Clay Miner. 35, 161–169.

Ehlmann, B.L., Mustard, J.F., Swayze, G.A., Clark, R.N., Bishop, J.L., Poulet, F., Marais, D.J.D., Roach, L.H., Milliken, R.E., Wray, J.J., Barnouin-Jha, O., Murchie, S.L., 2009. Identification of hydrated silicate minerals on Mars using MRO–CRISM: geologic context near Nili Fossae and implications for aqueous alteration. J. Geophys. Res. Planets 114, E00D08. doi:10.1029/2009JE003339.

Fergason, R.L., Christensen, P.R., Kieffer, H.H., 2006. High-resolution thermal inertia derived from the Thermal Emission Imaging System (THEMIS): thermal model and applications. JGR-Planets 111, E12004.

French, B.M., 1998. Traces of catastrophe: A Handbook of Shock-Metamorphic Effects in Terrestrial Meteorite Impact Structures. LPI Contribution No. 954, Lunar and Planetary Institute, Houston. 120 pp.

Glotch, T.D., Rogers, A.D., 2007. Evidence for aqueous deposition of hematite- and sulfate-rich light-toned layered deposits in Aureum and Iani Chaos, Mars. J. Geophys. Res. Planets 112, E06001. doi:10.1029/2006JE002863.

Glotch, T.D., Bandfield, J.L., Christensen, P.R., Calvin, W.M., McLennan, S.M., Clark, B.C., Rogers, A.D., Squyres, S.W., 2006. Mineralogy of the light-toned outcrop at Meridiani Planum as seen by the Miniature Thermal Emission Spectrometer and implications for its formation. J. Geophys. Res. Planets 111, E12S03.

Greeley, R., Guest, J.E., 1987. Geologic map of the eastern equatorial region of Mars. U. S. Geol. Surv. Misc. Invest. Ser. Map I-1802-B.

Griffes, J.L., Arvidson, R.E., Poulet, F., Gendrin, A., 2007. Geologic and spectral mapping of etched terrain deposits in northern Meridiani Planum. J. Geophys. Res. 112, E08S09.

Hamilton, V.E., Christensen, P.R., McSween, H.Y., Bandfield, J.L., 2003. Searching for the source regions of Martian meteorites using MGS TES: integrating Martian meteorites into the global distribution of igneous materials on Mars. Meteorit. Planet. Sci. 38, 871–885.

Hurowitz, J.A., McLennan, S.M., 2007. A similar to 3.5 Ga record of water-limited, acidic weathering conditions on Mars. Earth Planet. Sci. Lett. 260, 432–443.

Hurowitz, J.A., McLennan, S., Lindsley, D.H., Schoonen, M.A.A., 2005. Experimental epithermal alteration of synthetic Los Angeles Meteorite: implications for the origin of Martian soils and identification of hydrothermal sites on Mars. J. Geophys. Res. Planets 110. doi:10.1029/2005JE002391.

Johnson, J.R., Horz, F., Lucey, P.G., Christensen, P.R., 2002. Thermal infrared spectroscopy of experimentally shocked anorthosite and pyroxenite: implications for remote sensing of Mars. J. Geophys. Res. Planets 107. doi:10.1029/2001JE001517.

Johnson, J.R., Staid, M.I., Kraft, M.D., 2007. Thermal infrared spectroscopy and modeling of experimentally shocked basalts. Am. Mineralog. 92, 1148–1157.

Keller, W.D., 1955. The Principles of Chemical Weathering. Lucas Brothers Publishers, Columbia, Missouri, p. 88.

Kieffer, H.H., Martin, T.Z., Peterfreund, A.B., Jakosky, B.M., Miner, E.D., Palluconi, F.D., 1977. Thermal and albedo mapping of Mars during the Viking primary mission. J. Geophys. Res. 82, 4249–4291.

Koeppen, W.C., Hamilton, V.E., 2008. Global distribution, composition, and abundance of olivine on the surface of Mars from thermal infrared data. J. Geophys. Res. Planets 113, E05001.

Loughnan, F.C., 1969. Chemical Weathering of the Silicate Minerals. American Elsevier, New York.

Malin, M. C., 1976, Nature and Origin of Intercrater Plains on Mars, in Studies of the surface morphology of Mars: Unpub. Ph.D. dissertation thesis, California Institute of Technology.

McAdam, A.C., Zolotov, M.Y., Mironenko, M.V., Leshin, L.A., Sharp, T.G., 2006. Aqueous chemical weathering of a Mars analog lithology. Kinetic Modeling for a Ferrar Dolerite Composition. LPSC XXXVII.

McAdam, A.C., Zolotov, M.Y., Sharp, T.G., Leshin, L.A., 2008. Preferential low-pH dissolution of pyroxene in plagioclase–pyroxene mixtures: implications for Martian surface materials. Icarus 196, 90–96.

McDowell, M.L., Hamilton, V.E., 2009. Seeking phyllosilicates in thermal infrared data: a laboratory and Martian data case study. J. Geophys. Res. Planets 114, E06007. doi:10.1029/2008JE003317.

Michalski, J.R., Dobrea, E.Z.N., 2007. Evidence for a sedimentary origin of clay minerals in the Mawrth Vallis region, Mars. Geology 35, 951–954.

Michalski, J.R., Kraft, M.D., Sharp, T.G., Williams, L.B., Christensen, P.R., 2005. Mineralogical constraints on the high-silica Martian surface component observed by TES. Icarus 174, 161–177.

Mouginis-Mark, P., 1979. Martian fluidized crater morphology — variations with crater size, latitude, and target material. J. Geophys. Res. 84, 8011–8022.

Murchie, S., Green, R., Guinness, E., Hayes, J., Hash, C., Heffernan, K., Hemmler, J., Heyler, G., Humm, D., Hutcheson, J., Izenberg, N., Lee, R., Lees, J., Lohr, D., Malaret, E., Martin, T., McGovern, J.A., McGuire, P., Morris, R., Mustard, J., Pelkey, S., Rhodes, E., Robinson, M., Roush, T., Schaefer, E., Seagrave, G., Seelos, F., Silverglate, P., Slavney,

S., Smith, M., Shyong, W.J., Strohbehn, K., Taylor, H., Thompson, P., Tossman, B., Wirzburger, M., Wolff, M., 2007. Compact reconnaissance Imaging Spectrometer for Mars (CRISM) on Mars Reconnaissance Orbiter (MRO). J. Geophys. Res. Planets 112, E05S03.

Murchie, S.L., Mustard, J.F., Ehlmann, B.L., Milliken, R.E., Bishop, J.L., McKeown, N.K., Dobrea, E.Z.N., Seelos, F.P., Buczkowski, D.L., Wiseman, S.M., Arvidson, R.E., Wray, J.J., Swayze, G., Clark, R.N., Marais, D.J.D., McEwen, A.S., Bibring, J.P., 2009. A synthesis of Martian aqueous mineralogy after 1 Mars year of observations from the Mars Reconnaissance Orbiter. J. Geophys. Res. Planets 114, E00D06. doi:10.1029/2009JE003342.

Mustard, J.F., Murchie, S.L., Pelkey, S.M., Ehlmann, B.L., Milliken, R.E., Grant, J.A., Bibring, J.P., Poulet, F., Bishop, J., Dobrea, E.N., Roach, L., Seelos, F., Arvidson, R.E., Wiseman, S., Green, R., Hash, C., Humm, D., Malaret, E., McGovern, J.A., Seelos, K., Clancy, T., Clark, R., Des Marais, D., Izenberg, N., Knudson, A., Langevin, Y., Martin, T., McGuire, P., Morris, R., Robinson, M., Roush, T., Smith, M., Swayze, G., Taylor, H., Titus, T., Wolff, M., 2008. Hydrated silicate minerals on mars observed by the Mars reconnaissance orbiter CRISM instrument. Nature 454, 305–309.

Pelkey, S.M., Mustard, J.F., Murchie, S., Poulet, F., Bibring, J.P., Bishop, J.L., Izenberg, N., Seelos, F., Ehlmann, B.L., Roach, L.H., Milliken, R.E., Team, C., 2007a. CRISM observations of hydrated craters deposits in Terra Tyrrhena, Mars. Lunar Planet Sci. Abs. #1994.

Pelkey, S.M., Mustard, J.F., Murchie, S., Wolff, M., Smith, M., Milliken, R., Bibring, J.P., Gendrin, A., Poulet, F., Langevin, Y., Gondet, B., 2007b. CRISM multispectral summary products: parameterizing mineral diversity on Mars from reflectance. J. Geophys. Res. Planets 112, E08S14.

Poulet, F., Mangold, N., Platevoet, B., Bardintzeff, J.M., Sautter, V., Mustard, J.F., Bibring, J.P., Pinet, P., Langevin, Y., Gondet, B., Aleon-Toppani, A., 2009. Quantitative compositional analysis of Martian mafic regions using the MEx/OMEGA reflectance data 2. Petrological implications. Icarus 201, 84–101.

Rogers, A.D., Aharonson, O., 2008. Mineralogical composition of sands in Meridiani Planum determined from MER data and comparison to orbital measurements. J. Geophys. Res. Planets E06S14. doi:10.1029/2007JE002995.

Rogers, A.D., Christensen, P.R., 2007. Surface mineralogy of Martian low-albedo regions from MGS–TES data: implications for upper crustal evolution and surface alteration. J. Geophys. Res. Planets 112, E01003.

Rogers, A.D., Fergason R.L., submitted for publication. Geologic, thermophysical and compositional characteristics of surface units in Tyrrhena and Lapygia Terrae, Mars. JGR-Planets. November 2010.

Rogers, A.D., Christensen, P.R., Bandfield, J.L., 2005. Compositional heterogeneity of the ancient Martian crust: surface analysis of Ares Vallis bedrock with THEMIS and TES data. J. Geophys. Res. Planets 110. doi:10.1029/2005JE002399.

Rogers, A.D., Aharonson, O., Bandfield, J.L., 2008. Geologic context of in situ rocky exposures in Mare Serpentis, Mars: implications for crust and regolith evolution in the cratered highlands. Icarus 200, 446–462.

Ruff, S.W., Christensen, P.R., 2002. Bright and dark regions on Mars: particle size and mineralogical characteristics based on Thermal Emission Spectrometer data. J. Geophys. Res. Planets 107, 5127.

Ruff, S.W., Christensen, P.R., 2007. Basaltic andesite, altered basalt, and a TES-based search for smectite clay minerals on Mars. Geophys. Res. Lett. 34, L10204.

Schott, J., Berner, R.A., 1984. Dissolution mechanisms of pyroxenes and olivines during weathering. In: I., D.J. (Ed.), The Chemistry of Weathering. D. Reidel Publishing Company, Boston, pp. 35–54.

Seelos, F. P., Murchie, S. L., Pelkey, S. M., Seelos, K. D., and Team, C., 2007, CRISM Multispectral Survey Campaign — Status and Initial Mosaics: Lunar Planet. Sci. XXXVIII, Abs. 2336.

Seelos, K. D., Barnouin, O. S., and Team, C., 2010, Huygens Crater And The Highland Terrains In Western Tyrrhena Terra: Mineralogic Mapping With CRISM Data: 41st Lunar Planet Sci., Abs. # 2400.

Tanaka, K.L., Isbell, N.K., Scott, D.H., Greeley, R., Guest, J.E., 1988. The resurfacing history of Mars: a synthesis of digitized, Viking-based geology. Proc. Lunar Planet. Sci. Conf. 665–678.

Tornabene, L.L., McEwen, A.S., Osinski, G.R., Mouginis-Mark, P.J., Boyce, J.M., Williams, R.M.E., Wray, J.J., Grant, J.A., HiRISE Team, 2007. Impact Melting and the Role of Subsurface Volatiles: Implications for the Formation of Valley Networks and Phyllosilicate-Rich Lithologies on Early Mars. 7th International Mars Conference. #3288.

Tosca, N.J., McLennan, S.M., Lindsley, D.H., Schoonen, M.A.A., 2004. Acid-sulfate weathering of synthetic Martian basalt: the acid fog model revisited. J. Geophys. Res. Planets 109, E05003.

Wyatt, M.B., McSween, H.Y., Tanaka, K.L., Head, J.W., 2004. Global geologic context for rock types and surface alteration on Mars. Geology 32, 645–648.